Available online at www.sciencedirect.com
ScienceDirect
Ultramicroscopy 106 (2006) 1062–1068
ultramicroscopy
www.elsevier.com/locate/ultramic

Three-dimensional ADF imaging of individual atoms by through-focal series scanning transmission electron microscopy

Klaus van Benthem[a,*], Andrew R. Lupini[a], Mark P. Oxley[a,b], Scott D. Findlay[b], Leslie J. Allen[b], Stephen J. Pennycook[a]

[a]*Condensed Matter Sciences Division, Oak Ridge National Laboratory, Oak Ridge, TN 37831-6031, USA*
[b]*School of Physics, University of Melbourne, Victoria 3010, Australia*

Received 2 August 2005; received in revised form 9 November 2005; accepted 19 April 2006

Abstract

Aberration correction in scanning transmission electron microscopy has more than doubled the lateral resolution, greatly improving the visibility of individual impurity or dopant atoms. Depth resolution is increased five-fold, to the nanometer level. We show how a through-focal series of images enables single Hf atoms to be located inside an advanced gate dielectric device structure to a precision of better than $0.1 \times 0.1 \times 0.5$ nm. This depth sectioning method for three-dimensional characterization has potential applications to many other fields, including polycrystalline materials, catalysts and biological structures.
Published by Elsevier B.V.

Keywords: Optical slicing; STEM; ADF

1. Introduction

The distribution of single dopant atoms can dramatically influence the properties of semiconductors [1,2] and catalysts [3], which are arguably the two most important classes of modern materials. The detectability and lateral localization of such single atoms has been greatly improved by the recent development of aberration correction in the scanning transmission electron microscope (STEM) [4–6], which enables the formation of electron probes with diameters that can be as small as 0.6–0.8 Å [6]. An advantage of aberration correction is the increase in depth resolution by a reduced depth of field. This can be used for optically slicing the sample in a manner comparable to confocal optical microscopy [7].

Previous work imaging dopant atoms inside, e.g., semiconductor materials remains inconclusive about the distribution of dopant atoms in the third dimension [3,8]. Some studies conducted at lower resolution have used approximate matches to image simulations [8] or relied on statistical arguments to show that the imaged dopant atoms are in the bulk [9], neither of which is unequivocal proof of the location of the dopants. Varela and co-workers [10] have shown proof for a single La atom in the volume of a bulk solid by combining annular dark-field (ADF) STEM and electron energy-loss spectroscopy (EELS) in comparison to ADF and EELS image simulations. The proof of concept for a direct localization of individual atoms in three dimensions using a direct imaging technique was recently reported by van Benthem et al. [11]. In this study the vertical resolution limits are discussed in further detail. A comparison of ADF image intensities extracted from a through-focal series with image simulations is used to evaluate vertical resolution limits.

2. Methodology

2.1. Three-dimensional (3D) imaging

Nellist and co-workers reported an electron probe size of 0.78 Å by imaging {4 4 0} lattice planes in a silicon crystal [6] using an aberration-corrected STEM. This lateral resolution limit provides single-atom resolution and

*Corresponding author.
E-mail address: benthem@ornl.gov (K. van Benthem).

0304-3991/$ - see front matter Published by Elsevier B.V.
doi:10.1016/j.ultramic.2006.04.020

sensitivity in the conventional two-dimensional (2D) projection view [3]. The lateral resolution limit or spot size is given by $\delta_s = \lambda/\alpha$, where λ is the wavelength of the incident electrons and α is the illumination semi-angle. Based on purely geometric considerations, the depth of field T may be written as [12]

$$T \approx \frac{\delta_s}{\alpha} = \frac{\lambda}{\alpha^2}. \quad (1)$$

One of the main benefits of aberration correction in the STEM is that larger illumination angles can be used [5] without degrading the spatial resolution due to significant lens aberrations associated with higher angles. Thus, the increased spatial resolution together with the availability of larger illumination angles leads to a strong decrease in the depth of field, following Eq. (1). This effect is demonstrated in Fig. 1, which shows electron probe profiles as a function of defocus for three different cases: (a) an uncorrected 300 kV VG HB603 U dedicated STEM ($C_3 = C_s = 1$ mm, $\alpha = 9.5$ mrad), and the aberration-corrected STEM ($C_s = -37\,\mu$m) of the same type for (b) $\alpha = 12$ mrad and (c) $\alpha = 23$ mrad. In all three cases, the same values were used for the electron gun energy spread $\Delta E = 0.3$ eV, the chromatic aberration coefficient $C_C = 1.6$ mm and the higher-order symmetric lens aberration coefficient $C_5 = 100$ mm. Non-symmetric higher-order aberrations were not considered.

Fig. 2 shows a sketch of two atoms vertically separated by $1\times$, $1.75\times$ and $2\times$ the depth of field T. At each atom position, a vertical probe profile is plotted. The dotted lines show the corresponding superposition of the adjacent profiles. For a vertical separation of $1.75T$, the two atoms become distinguishable. At a distance of $2T$, the image intensity (dotted line) drops to about 80% of the maximum intensity between the two atoms. Therefore, we can formulate an analogy for the vertical resolution T_R similar to the lateral resolution limit following the Raleigh criterion, in which two atoms in the same lateral position are resolved by depth sectioning when their vertical separation is at least the distance between the waist and the first minimum of the electron probe intensity distribution [13]. Hence, a vertical resolution limit T_R is proposed as follows

$$T_R = 2T \approx 2\frac{\delta_s}{\alpha} = 2\frac{\lambda}{\alpha^2}. \quad (2)$$

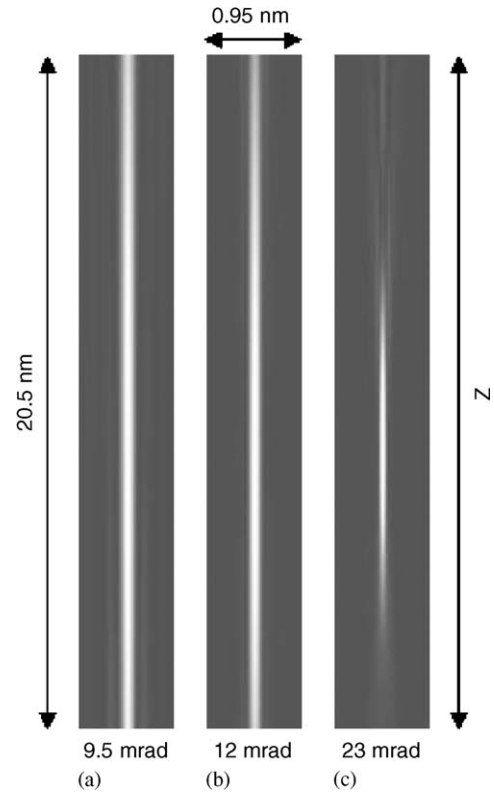

Fig. 1. (a) The electron probe intensity profile for an uncorrected 300 kV STEM using a typical convergence angle of 9.5 mrad. Probe profiles are also plotted for the aberration-corrected microscope for convergence angles of (b) 12 mrad and (c) 23 mrad.

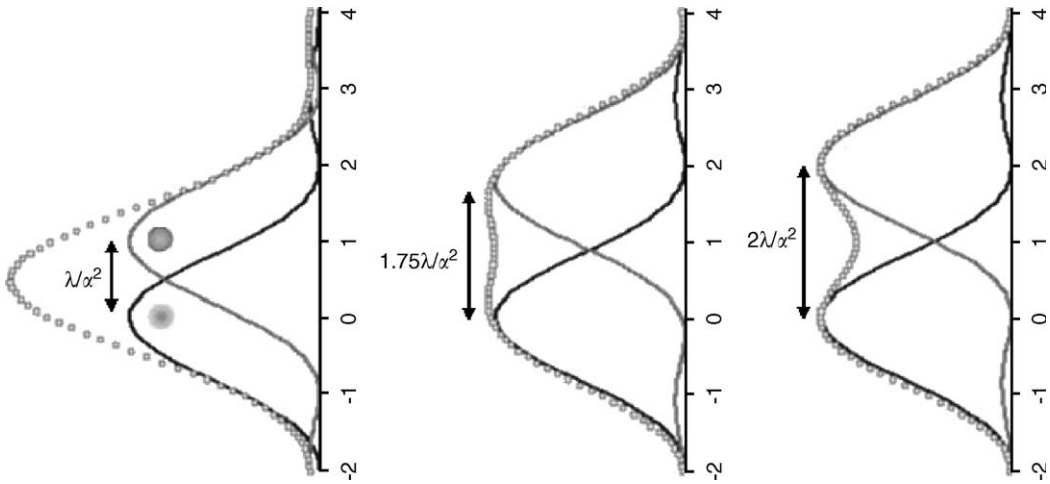

Fig. 2. Sketch of two isolated atoms vertically separated by $1\times$, $1.75\times$ and $2\times$ the depth of field $T = \lambda/\alpha$. At the position of each atom, a simulated vertical probe profile is plotted. The dotted line is a superposition of the two corresponding profiles.

The Oak Ridge VG HB603 U aberration-corrected STEM is capable of providing electron probe diameters of 0.78 Å [6] for a convergence semi-angle of $\alpha = 23$ mrad. This compares to $\delta_s = 1.28$ Å and $\alpha = 9.5$ mrad in the uncorrected case [14]. Therefore, due to the correction of lens aberrations, the vertical resolution limit T_R was improved from about 29 nm to 6.8 nm.

By recording images at different defocus values, it is then possible to "slice" through the sample in a manner comparable to that used in confocal optical microscopy [7]. Fig. 3 shows the principle of a through-focal series acquisition. The first image is taken with the electron beam focused in one particular plane. Then, the focus is changed by a fixed amount and the second image is recorded. By repeating this multiple times using fixed focus increments, the sample is optically sliced and an image stack is recorded. This image stack then contains full 3D information about the imaged structure, which can be used for further 3D reconstructions. First proofs of concept of this technique were recently published in Refs. [3] and [7]. Here we discuss the apparent resolution limits and visibility of single isolated atoms in three dimensions in greater detail.

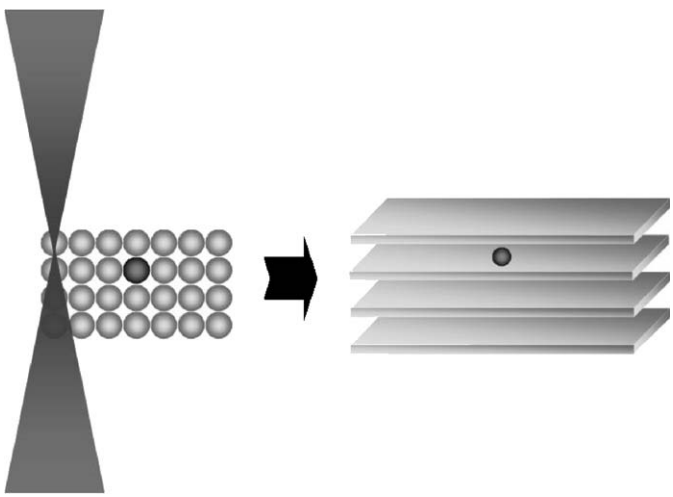

Fig. 3. Sketch of the basic principle for optically sectioning a sample by acquisition of a through-focal series.

2.2. Experimental details

About 3 nm thick HfO_2 films were deposited on silicon substrates using atomic layer deposition at a temperature of 320 °C. Afterwards, the HfO_2/SiO_2 interface was rapid-thermal annealed at 950 °C for 30 s in N_2 and then capped with undoped polycrystalline Si using chemical vapor deposition. To avoid artifacts from ion milling, samples were prepared for cross-sectional STEM purely by mechanical polishing. The VG Microscope HB603 U dedicated STEM at Oak Ridge National Laboratory, which is equipped with a third-order aberration corrector (Nion Co. [15]) for the probe-forming lenses, was used for the reported investigations. The microscope was operated at a 300 kV accelerating voltage and an illumination semi-angle of 23 mrad was used. The electron probe size was measured to be below 0.1 nm. The electron beam current was less than 20 pA. Recorded frame sizes were 512×512 pixels. Dwell times were 32 microseconds/pixel, corresponding to an acquisition time of 8 s per frame. To avoid contamination effects during acquisition times, the sample was heat treated for 30 min at roughly 150 °C under UHV conditions in the airlock of the microscope. A through-focal series containing 41 images was recorded with a focal step size of 0.5 nm, controlled by the objective lens current. After recording a full through-focal series, one additional frame was acquired from the same specimen area to verify that no beam damage or contamination has occurred during the acquisition. None of the data presented has been Fourier filtered.

3. Results

In the electron microscope, the Si substrate was oriented in a ⟨1 1 0⟩ zone–axis orientation, i.e., the optical axis is parallel to the (0 0 1) planes of the silicon crystal. Fig. 4 shows an ADF and a bright-field (BF) STEM image

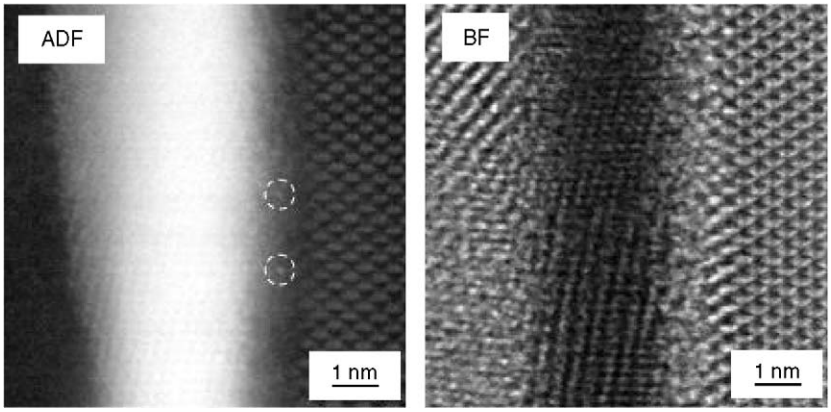

Fig. 4. ADF and BF images recorded simultaneously from the high-k dielectric stack. In the ADF image, bright contrast is observed (circled), which represents isolated Hf atoms within an SiO_2 interlayer. The amorphous SiO_2 interlayer can clearly be observed in the BF image.

recorded simultaneously from the Si/HfO_2 interface. The micrographs clearly indicate a thermally grown amorphous SiO_2 interlayer between the Si substrate and the polycrystalline HfO_2 film. EELS measurements confirmed the presence of SiO_2. At high magnification, ADF STEM images revealed the presence of single Hf atoms within the amorphous SiO_2 interlayer. Fig. 5 shows nine images extracted from a through-focal series recorded from the same specimen area in less than 5 min. At various defocus values, single Hf atoms come into focus in 3–5 frames each, corresponding to intervals of 1.5–2.5 nm in depth (see, for instance, the white circles in Fig. 5). No evidence of beam damage effects was observed in micrographs recorded from the same areas immediately after the through-focal series acquisition.

To demonstrate the location of one of the Hf atoms marked in Fig. 5, Fig. 6 shows a slice view of the 3D data cube. The image in the *x–y* plane reveals the polycrystalline HfO_2 layer separated from the Si substrate by a less than 1-nm-thick amorphous SiO_2 layer. The single Hf atom visible about half way through the *z*-range in the *x–y* plane is observed in the *x–z* and the *y–z* planes as a single atom. It has to be noted that the voxels (volume picture elements) in this data set are not cubic but cuboid due to the limited number of acquired frames in the vertical direction compared to the high number of pixels in the lateral directions. The voxel size is about 0.2 Å × 0.2 Å × 5 Å in the *x*-, *y*- and *z*-directions, respectively.

Intensity line profiles were extracted from the 3D data set as shown in Fig. 7. Atom columns in bulk Si exhibit excess intensities of about 800–900 counts over a background of roughly 3000 counts between the Si columns (no dark current level was subtracted). Each single Hf atom embedded in the SiO_2 interlayer provides up to about 850 counts above a local background level of roughly 4200–4300 counts, as displayed in Fig. 7. The exact number of counts depends on the integration width used for extracting the line profile. Note that the intensity background in the SiO_2 layer is highly non-uniform (cf. slope in Fig. 7) and is formed by out-of-focus contributions of other single embedded Hf atoms, bulk Si columns and the adjacent HfO_2 film. ADF image intensity profiles were extracted from each acquired frame across five representative single Hf atoms. The average background intensity in the vicinity of a single Hf atom was subtracted from the maximum image intensity due to the present atom. This excess intensity is plotted in Fig. 8 as a function of defocus Δf and depth inside the sample *d*. For the used imaging conditions, balancing the aberrations leads to maximal probe intensity at a defocus value of $\Delta f = 20$ Å overfocus. Hence, Δf and the depth inside the sample are related by $d = 20 - \Delta f$. The two profiles located around defocus values of 20 and −40 Å represent the outermost isolated Hf atoms found among a total of 65 atoms throughout the entire 3D data set. Hence, it is assumed that these two atoms are located close to or on the top and bottom surfaces of the specimen.

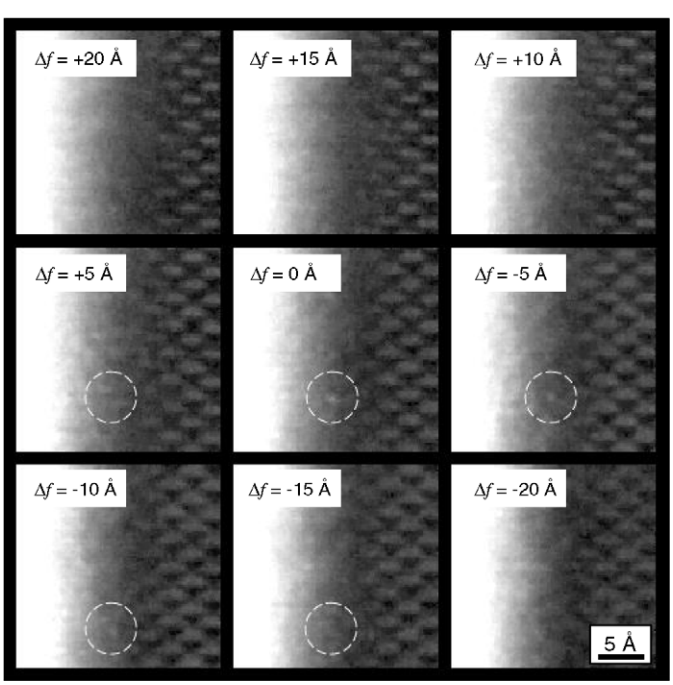

Fig. 5. Nine consecutive micrographs extracted from a 41-image through-focal series. The white circles mark one single Hf atom coming into focus within a limited focal interval. Micrographs are displayed using a non-linear contrast scale.

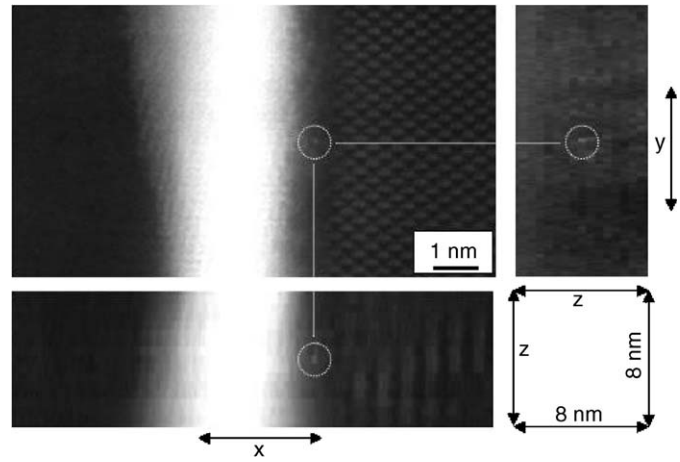

Fig. 6. Three different views through the 3D data set. The *y–z* and the *x–z* slices clearly show the location of the single Hf atom observed in Fig. 5 in the vertical direction. The voxel sizes are 0.2 Å × 0.2 Å × 5 Å.

4. Discussion

Before aberration correction, STEM led to a 2D projection of a truly 3D structure. As demonstrated in Fig. 1, the reduced depth of field due to the availability of larger illumination angles without picking up large amounts of third-order lens aberrations concentrates image intensities vertically in a smaller focus interval. However, since the aberration correction is performed by balancing all higher-order lens aberrations, the vertical probe profile becomes somewhat asymmetric [13]. The overall reduced

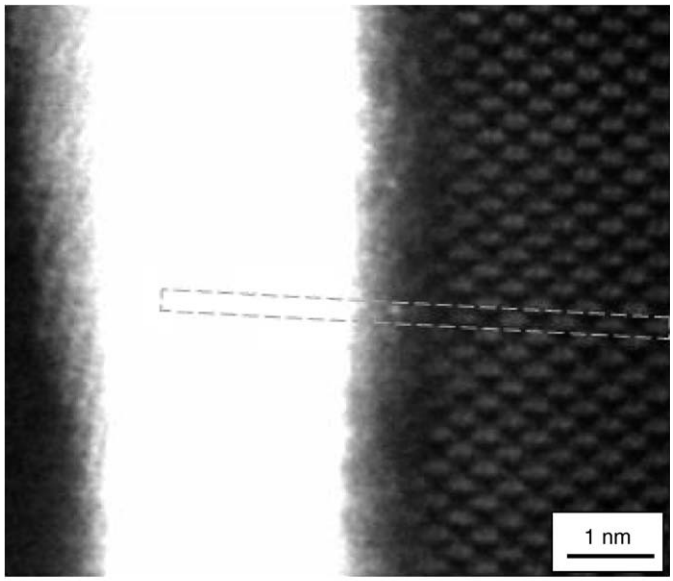

(a)

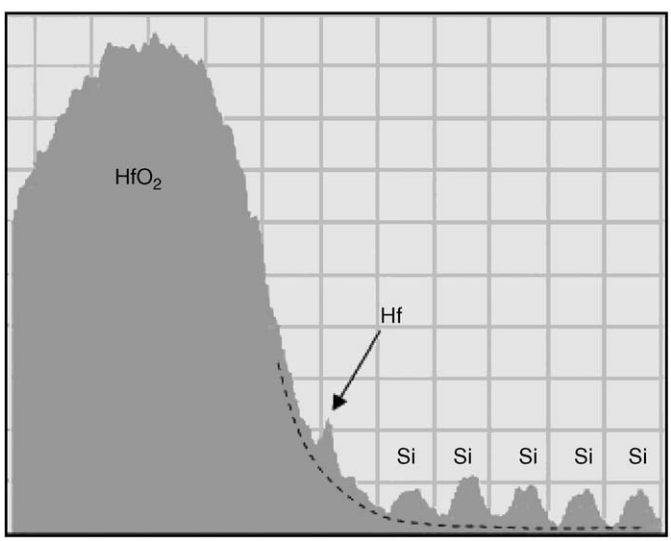

(b)

Fig. 7. (a) An ADF image taken from a through-focal series. As indicated in (a), an intensity line profile across the $HfO_2/SiO_2/Si$ interface was extracted, which is plotted in (b). The profile demonstrates the largely non-uniform intensity background for the SiO_2 layer.

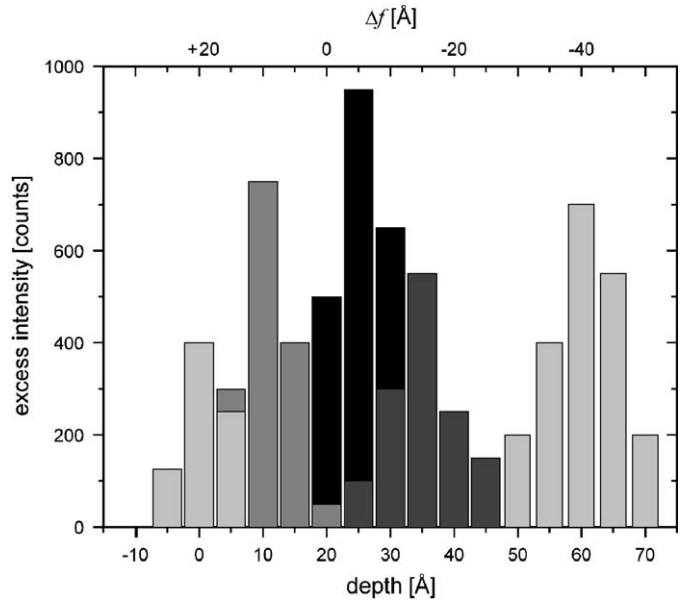

Fig. 8. Excess image intensities due to five individual Hf atoms. Intensity profiles for the different atoms are plotted with different grey shadings. The vertical interval in which a total of 65 single Hf atoms are observed is limited by the two outermost profiles at 0 and 60 Å depth.

focal depth leads to an increased vertical resolution when optically slicing the sample by acquiring a through-focal series. Even though the exact vertical probe profile is difficult to determine experimentally for reconstruction or deconvolution purposes, the focal series acquisition provides a new 3D imaging strategy in STEM. In the case of heavy stray atoms embedded in a matrix with low atomic number, the vertical location of these atoms becomes possible with a precision significantly higher than the actual vertical resolution limit.

Figs. 4 and 5 show that single Hf atoms come into focus and, thus, are visible only in a very limited focus interval of about 2.5 nm. This is for the first time a *direct* proof that dopant or impurity atoms are located *in the volume* of the sample rather than on either of the two surfaces. As already mentioned, previous investigations done at lower resolution were always based on statistical arguments or quantitative image simulations [8–10]. From the position of the two outermost intensity profiles found throughout the image stack (Fig. 8), the sample thickness can be estimated to be 6 ± 1 nm. All other profiles appear within the above-mentioned defocus interval. An analysis of the intensity profiles of all other single Hf atoms within the SiO_2 interlayer shows that the stray atoms are randomly distributed in the vertical direction. From Fig. 8, it is evident that the *precision* with which the depth of such isolated atoms can be located is better than ± 0.5 nm, because the location of the intensity maximum can be determined by fitting the intensity profile. This is a concept which is also extensively used in confocal optical microscopy [7].

Figs. 9(a) and (b) show simulated intensity line profiles across a single Hf atom in SiO_2 and across atom columns in bulk Si in $\langle 1\,1\,0 \rangle$ zone–axis orientation, respectively. The calculations were performed using a multislice approach for a 6.4-nm-thick sample with the dopant positioned about 2.6 nm below the surface. The exact values as in the experiment were used for C_s and C_5. For the given aperture ($\alpha = 23$ mrad), the absolute defocus value is 21 Å. For the Si atom columns (Fig. 9(b)), the maximum signal strength derives from a defocus of -10 Å. In a geometric model, this corresponds to the electron beam waist positioned 31 Å into the sample, i.e., halfway through the sample thickness where the overlap of probe intensity (cf. Fig. 1) and the effective scattering potential become maximal. For the single Hf atom, the maximum signal strength derives from

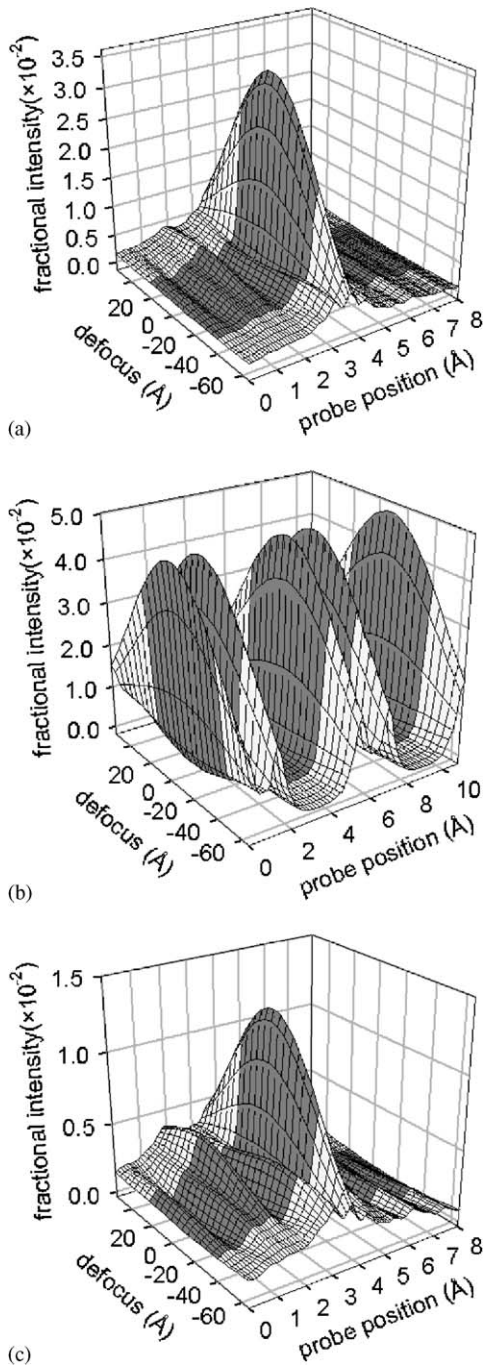

Fig. 9. Intensity line profiles extracted from ADF image simulations (a) for isolated Hf atoms embedded in SiO_2, and (b) for bulk Si in ⟨1 1 0⟩ zone–axis orientation. (c) An intensity profile simulated as (a) except that Zr is used instead of Hf. In all three panels, the vacuum region above and below the sample is color coded in yellow (online), i.e., brighter intensity (in print).

a defocus value of −5 Å, corresponding to the beam waist located 26 Å into the sample.

The simulations reveal comparable image intensities for single Hf atoms and Si columns, reproducing the experimental observation. Although image intensities of isolated Hf atoms in SiO_2 are comparable to those of atomic columns in bulk Si, the signal-to-background ratio for Hf atoms is considerably smaller because of the larger background. Furthermore, the focal width of the Si column signal in Fig. 9(b) depends on the thickness of the sample. While the Hf signal approaches zero intensity near the two surfaces, the Si signal is still substantial (about one quarter of its maximum) even in the vacuum above and below the sample, since parts of the Si columns are always in focus. This clearly demonstrates that the bright intensities within the SiO_2 interlayer are due to single Hf atoms rather than isolated Si columns.

The large background is formed by out-of-focus contributions from the SiO_2, other isolated Hf atoms present at different depths, the nearby HfO_2 film and the nearby Si columns in the bulk Si. Out-of-focus contributions of a single Hf atom can contribute to the background by half of its in-focus intensity, i.e., more than 200 counts (cf. Fig. 8). Poisson statistics suggest that there will be a shot noise contribution of at least 50–100 counts. Hence, the background level can be approximately 50% of the maximum in-focus intensity for single Hf atoms embedded in SiO_2. This suggests that if single Zr atoms, which are about three times dimmer than single Hf atoms, are present, they would not be visible above the noise under the imaging conditions used. This observation agrees well with results obtained from ADF image simulations for a single Zr atom in SiO_2 compared to a column of Si atoms (Fig. 9(c)).

The simulated image intensity profiles show a full-width at half-maximum (FWHM) of 6.5 nm above the background level. For the simulations, only a simple model of an isolated interstitial Hf atom embedded in SiO_2 was used, without consideration of the nearby Si substrate and the HfO_2 film. Therefore, the out-of-focus intensity background does not represent the experimentally observed intensity background.

It is initially surprising that the FWHM of the excess intensity profiles in Fig. 8 appear to be significantly smaller than the expected vertical resolution; however, this is not really the case. In the previous paragraph, we demonstrated that about 50% of the image intensity from the isolated Hf atoms is obscured by the background due to significant out-of-focus contributions. Therefore, only about the upper 50% of values in Fig. 8 are detectable above the background. In other words, the intensity contribution is present in more frames than those in which we can reliably detect it. Hence, the experimentally observed FWHM in Fig. 8 is decreased by at least a factor of two. Therefore, the vertical resolution of our technique is really of the order of 6–8 nm, although the isolated Hf atoms appear cigar shaped with an extent of about 2 nm due to the limited signal-to-background statistics. Recently, Pennycook and co-workers have shown that indeed a larger vertical FWHM is observed when isolated atoms are imaged against a more uniform background (under otherwise similar conditions), such as for Pt atoms on carbon [13].

5. Conclusion

In the present study we have shown that aberration correction of the probe-forming lenses in a dedicated STEM does not only lead to a reduction in the lateral spatial resolution but also significantly reduces the depth of field, i.e., the vertical resolution. Available resolution limits are in the sub-Angstrom regime laterally and in the 6–7 nm regime vertically. A through-focal series acquisition then provides the possibility to optically slice the specimen. The recorded image stacks can be used for a 3D reconstruction of the investigated structure. Here, it was shown that it is even possible to image isolated heavy atoms in an amorphous matrix with a low atomic number. Furthermore, it has to be noted that it is possible to obtain the depth of, e.g., a single atom with a *precision* that is by far *better* than the vertical FWHM of the probe, because that is determined by the sampling and the signal-to-background ratio, not just the resolution.

So far, only third-order aberration correctors have been used. In the future, the availability of corrector elements to suppress fifth-order lens aberrations will further decrease the depth of field and, hence, increase the vertical resolution limits to about 1 or 2 nm. Hence it is plausible that the acquisition of through-focal series becomes necessary to guarantee the best possible imaging conditions at typical specimen thicknesses in excess of 10 nm. The assumption that STEM is always a 2D projection of the transmitted specimen is no longer valid.

Acknowledgements

This research was sponsored by the Laboratory Directed Research and Development Program of ORNL, managed by UT-Battelle, LLC, for the US Department of Energy under Contract No. DE-AC05-00OR22725 and by an appointment to the ORNL Postdoctoral Research Program administered jointly by ORNL and ORISE. KvB greatly appreciates funding from the Alexander-von-Humboldt Foundation. LJA and MPO acknowledge support from the Australian Research Council.

References

[1] P.A. Packan, Science 285 (1999) 2079.
[2] G. Moore, Electronics 38 (1965).
[3] S. Wang, A.Y. Borisevich, S.N. Rashkeev, M.V. Glazoff, K. Sohlberg, S.J. Pennycook, S.T. Pantelides, Nature Mater. 3 (2004) 143.
[4] P.E. Batson, N. Dellby, O.L. Krivanek, Nature 418 (2002) 617.
[5] O.L. Krivanek, P.D. Nellist, N. Dellby, M.F. Murfitt, Z.S. Szilagyi, Ultramicroscopy 96 (2003) 229.
[6] P.D. Nellist, M.F. Chisholm, N. Dellby, O.L. Krivanek, M.F. Murfitt, Z.S. Szilagyi, A.R. Lupini, A.Y. Borisevich, W.H. Sides, S.J. Pennycook, Science 305 (2004) 1741.
[7] A.R. Lupini, M. Varela, A.Y. Borisevich, S.M. Travaglini, S.J. Pennycook, Inst. Phys. Conf. Ser. 179 (2004) 211.
[8] P.M. Voyles, D.A. Muller, J.L. Grazul, P.H. Citrin, H.-J.L. Gossmann, Nature 416 (2002) 826.
[9] A.R. Lupini, S.J. Pennycook, Ultramicroscopy 96 (2003) 313.
[10] M. Varela, S.D. Findlay, A.R. Lupini, H.M. Christen, A.Y. Borisevich, N. Dellby, O.L. Krivanek, P.D. Nellist, M.P. Oxley, L.J. Allen, S.J. Pennycook, Phys. Rev. Lett. 92 (2004) 095502.
[11] K. van Benthem, A.R. Lupini, M. Kim, H.S. Baik, S.J. Doh, J.-H. Lee, M.P. Oxley, S.D. Findlay, L.J. Allen, S.J. Pennycook, Appl. Phys. Lett. 87 (2005) 034104.
[12] L. Reimer, Transmission Electron Microscopy, Springer, Berlin, 1997.
[13] A.Y. Borisevich, A.R. Lupini, S.J. Pennycook, Proc. Natl. Acad. Sci. 103 (2006) 3044.
[14] P.D. Nellist, S.J. Pennycook, J. Microsc. 190 (1998) 159.
[15] www.nion.com